Stochastic Interpretation of CO_2-Brine Primary Displacement in Heterogeneous Carbonate Rocks

Omidreza Amrollahinasab[1], *Boris Jammernegg*[1], Siroos Azizmohammadi[1] and *Holger Ott*[1,*]

[1]Department Petroleum Engineering, Montanuniversität Leoben, 8700 Leoben, Austria

Abstract. CO_2 migration is affected by rock heterogeneity but is not reflected in the relative permeability ($k_r(S_w)$) and capillary pressure ($P_c(S_w)$) saturation functions measured by special core analysis (SCAL). We present a first step to an upscaling workflow that combines state-of-the-art SCAL interpretations with continuum-scale experiments on the next larger scale where heterogeneities dictate CO_2-brine displacement. By numerical interpretation using 1D homogeneous and 3D heterogeneous simulation domains, we show that an effectively upscaled $k_r(S_w)$ is substantially out of the uncertainty range of classical SCAL measurements used for $k_r(S_w)$ quantification. Alternatively, by including porosity, permeability and capillary heterogeneity, the SCAL-derived relative permeability is well applied. However, this effectively corresponds to downscaling and is therefore of little value for reservoir simulations. Our results demonstrate the following: (a) simple USS experiments can be used to investigate the influence of capillary heterogeneity on $k_r(S_w)$, and (b) a rigorous upscaling procedure including rock heterogeneity on various scales is needed to use standard workflows such as special core analysis for CCS developments in carbonates.

1 Introduction

Accurate prediction of fluid flow and two-phase displacements in subsurface reservoirs is essential for a range of applications, including hydrocarbon extraction and geological CO_2 storage. However, the unexpected migration of carbon dioxide in CO_2 injection operations highlights the need to improve our understanding of the underlying mechanisms, particularly in heterogeneous reservoirs [1–4]. Rock formations are typically heterogeneous on various scales. This poses a major challenge for the design and interpretation of measurements of multiphase flow properties, as the definition of a representative elementary volume (REV) depends not only on the scales of heterogeneity versus the sample size but also on the nature of the measured property [5–8]. The dependency of capillary forces on heterogeneity results in a local variation in saturation states during immiscible displacements, referred to as 'capillary heterogeneity'. Conceptionally, this effect can be described through the spatial variability of the capillary-pressure saturation function [9]. This phenomenon has practical consequences, as the measurement of multiphase flow parameters may depend on the measurement scale [10–12]. For example, rock heterogeneity at the submeter scale, such as laminations and bedding, can significantly impact fluid flow properties and must be considered to successfully model and predict fluid flow at larger scales [12–14]. The effect can be particularly strong in multiscale heterogeneous carbonates and when significant viscosity contrasts are observed (e.g., CO2-brine displacements).

Conventional reservoir simulation workflows naturally cannot explicitly represent the impact of small-scale heterogeneity on multiphase flow properties, such as relative permeability and capillary pressure characteristics [15–17]. Relative permeability is a key parameter that controls the displacement and sweep efficiency in immiscible displacement. The main challenge in characterizing relative permeability is that laboratory and special core analysis (SCAL) measurements are usually performed on homogeneous samples that do not accurately represent the average property at the size of the discretization of a reservoir model. To illustrate this point, we can compare the size of a SCAL plug, which is on the order of centimeters, to a typical grid block in a reservoir simulation, which may be orders of magnitude larger. The information we have from the subsurface is scarce, and the understanding of the upscaling workflow from the homogeneous rock–fluid properties (SCAL) to the heterogeneous next scale is limited. Therefore, different approaches have been developed to characterize capillary heterogeneity within rock cores [14, 18–26], but uncertainty remains in characterizing more complex rocks typical of subsurface reservoirs across the fractional flow curve and for different flow rates [27, 28].

Multiscale workflow from the micron (pore) scale to the meter scale, offer new opportunities to systematically upscale multiphase flow for reservoir application purposes [29]. These workflows combine laboratory-based characterization techniques, such as core flooding with in situ imaging methods on various scales and digital rock physics, with upscaling schemes that account for capillary pressure heterogeneity. With rigorous upscaling, small-scale effects can be incorporated into continuum-scale models when interpreted by numerical modeling using an optimization routine; effective petrophysical parameters and relative permeability saturation functions can be calculated, including their uncertainties [7, 19, 29–32]. However, implementing

* Corresponding author: holger.ott@unileoben.ac.at

sample heterogeneity for interpretation of relative permeability refers to a downscaling rather than an upscaling as long as the heterogeneity is not represented in a grid block of a reservoir model.
A well-studied candidate rock sample with a high degree of heterogeneity is Estaillades limestone. Studies have shown that relative permeability saturation functions derived from classical SCAL experiments do not adequately represent the behavior of larger rock volumes that are 12 times the volume of the samples typically used in SCAL studies, particularly when these volumes encompass 3-inch diameter cores [33][30].
In a prior study [30], we developed a comprehensive stochastic SCAL analysis workflow and applied it to steady-state and centrifuge experimental data on decane-brine primary drainage in Estaillades. The analysis yielded confidence intervals of combined measurements and sample-to-sample variations [30].

In the present study, building upon our previous work [30], we perform two key investigations depicted in **Fig *1***:

1- We conduct a comparative analysis between full stochastic interpretations of SCAL data (steady state and centrifuge) and larger-scale unsteady state (USS) core flood experiments using 1D homogeneous simulation domains. By presuming homogeneity, the analysis of the USS experiment yields the upscaled $k_r(S_w)$, inclusive of the confidence interval.

2- We incorporate the 3D porosity profile as determined by X-ray computed tomography (CT) and the resulting permeability and capillary heterogeneity. By history matching the USS experiment on the 3D heterogeneous domain, we aim to determine the true $k_r(S_w)$ and shed light on the impact of heterogeneity on the investigated scale.

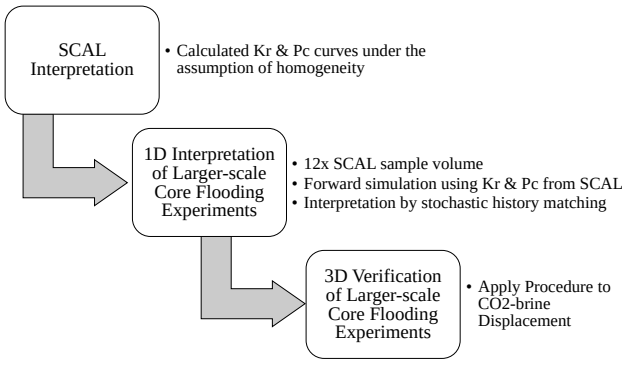

Fig 1. Workflow of the study. This diagram illustrates the progressive approach taken in this research, starting from the homogeneous analysis through to the 3D heterogeneous simulation. It depicts the distinct steps and methodologies employed at each stage, underlining the complex interplay between experimental work, numerical interpretation, and the investigation of heterogeneity effects on relative permeability saturation functions.

These investigations are intended to delineate the influence of rock heterogeneity on relative permeability measures and capillary pressure, thereby improving our understanding and predictive capability of CO_2-brine displacement in heterogeneous carbonate rocks.
To study the effect of heterogeneity on relative permeability, we analyze decane-brine and CO_2-brine unsteady-state experiments. The first serves as a water-wet reference case that directly refers to the earlier steady-state measurements, and the second is the system under investigation. Heterogeneity is introduced step by step by first considering a 1D homogeneous simulation domain, then a 1D heterogeneous domain, and finally the actual 3D heterogeneous domain. For 1D homogeneous cases, a full stochastic analysis is feasible and thus, carried out. For the 1D heterogeneous domain, simple history matching is performed to derive the base case $k_r(S_w)$, which is also used for the 3D simulations, considering the full set of experimental saturation data. By progressively increasing the complexity of the fluid pairs and simulation domains, we ensure that the approach is robust and applicable to a wide range of scenarios. This methodology will provide valuable insights into the validity and limitations of the current SCAL procedures and pave the way for the development of alternative methods and upscaling workflows for calculating saturation functions.

2 Experimental and Numerical Methods

The work was performed using experimental results published by [33]. The experiments were performed on Estaillades (EST) limestone samples with a length of 15 cm and a diameter of 7.5 cm. The average rock porosity and permeability were experimentally derived to $\phi = 0.297$ and $K = 260$ mD, respectively.
The experiments were performed at elevated pressure and temperature conditions of 100 bar and 50°C, referring to approximately 1000 m reservoir depth at which the injected CO_2 is in the supercritical state (sc). To investigate the primary displacement process of brine by CO_2, the sample was first saturated to $S_w = 1$ and then flooded with $scCO_2$. A reference measurement was performed with decane as the injection phase; the decane-brine experiments serve as a reference and can directly be compared to the earlier SCAL interpretation since SCAL measurements were performed with the same pair of fluids and on rock samples from the same block of the Estaillades outcrop. The flooding experiments were conducted under unsteady-state (USS) conditions, employing distinct constant injection rates for decane and CO_2. Specifically, a liquid injection rate of 0.25 ml/min was used for both decane and CO2 at the pump. However, due to the unique characteristics of CO2, where it changes from liquid form to supercritical state after injection, a volume correction is applied. As a result, the effective injection rate for CO2 is calculated to be 0.44 ml/min. This difference in effective rates considers the transformation of CO2 from its liquid form to its supercritical state. This process allows a fair comparison and interpretation of the displacement processes between the reference decane-brine and the CO2-brine system. During the experiments, the pressure drop was measured, and the upfront 3D porosity

profiles and 3D saturation profiles were taken by difference imaging via in situ medical CT scanning. Production curves were derived from CT saturation monitoring. The 3D saturation profiles are shown in **Fig. 2** for the decane-brine displacement (top row) and the CO2-brine displacement (bottom row) with the invading fluid in orange and the initial rock-fluid system as a semitransparent background. Further experimental details can be found in [33].

The simulation methodology developed in this study uses the MATLAB Reservoir Simulation Toolbox (MRST) to simulate immiscible displacement of fluids in reservoirs, operating under the assumption of incompressible flow. This process effectively employs Darcy's law for momentum balance and material balance equations to describe the fluid flow through porous media. Upon completion of the simulation, we turn to 'history matching'. This is a process of adjusting the simulation parameters until the simulated results closely mirror the observed experimental data. For this optimization problem, we employ MATLAB's global optimization module, which makes use of genetic or active-set algorithms for a constrained nonlinear optimization. After achieving the best match, we further utilize the Markov Chain Monte Carlo (MCMC) method, specifically the Delayed-Rejection Adaptive-Metropolis (DRAM) algorithm, to examine the response surface around the optimal solution and determine its sensitivity. The DRAM approach is fully automated and enhances the efficiency of the MCMC sampler, which is especially valuable when dealing with high-dimensional problems inherent in the saturation functions' high number of parameters. This combination of numerical techniques and simulation methods provides a robust solution for history matching and uncertainty analysis. The methodology is discussed in [30] and is applied to unsteady state experiments in the present study. The introduction of rock heterogeneity is discussed in a separate chapter below.

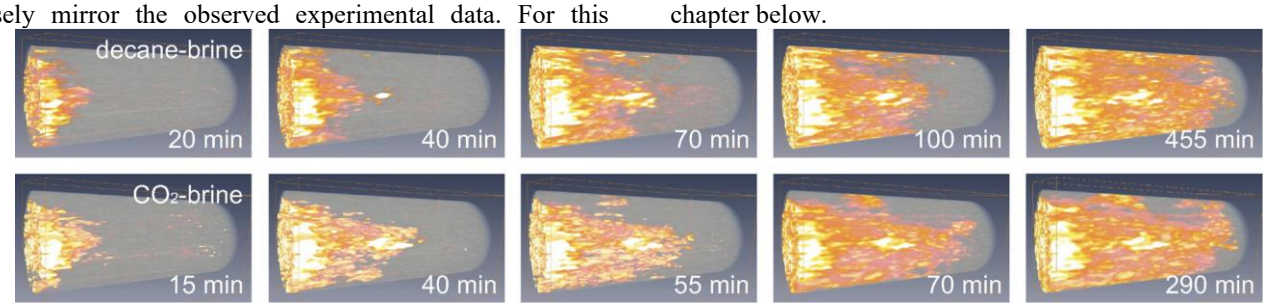

Fig. 2. CT time sequences of the decane–brine (top) and CO2–brine (bottom) experiments. The decane and CO2 saturation distributions are illustrated in orange, and the initial rock-fluid system is displayed as a semitransparent background. Note that the threshold setting for the saturation is comparable but arbitrary to highlight heterogeneity in the saturation distribution.

3 Interpretation Assuming Homogeneity

A key assumption in classical SCAL interpretation is that the samples are considered homogeneous, resulting in a simple 1D homogenous simulation domain. This assumption requires careful sample selection and reasonably small samples with a volume that can be considered a representative elementary volume (REV). The data once interpreted are therefore single sets of relative permeability and capillary pressure saturation functions that do not need further interpretation. In reservoir simulations, such $k_r(S_w)$ and $P_c(S_w)$ saturation functions are typically assigned to rock types with heterogeneity being accounted for by a Laverett-J scaling of the $P_c(S_w)$ [34]. In any case, in a single grid block, only one $k_r(S_w)$ and $P_c(S_w)$ saturation function is assigned, implicitly considering the grid block as homogeneous.

Compared to small-scale SCAL experiments, larger-scale core flooding is typically affected by the size and heterogeneity of the sample, and sweep effects are observed [14, 33]. Now, there are two options for numerically interpreting the data: (a) introducing rock heterogeneity of various properties into the simulation model, resulting in "true" saturation functions, and (b) ignoring rock heterogeneity, i.e., considering the rock domain as homogeneous and representative. In the latter scenario, where rock heterogeneity is ignored, we do not anticipate obtaining the same relative permeability. Instead, we expect to derive an effective $k_r(S_w)$ that accurately represents the investigated volume, a value we consider the upscaled $k_r(S_w)$. This upscaled value, however, might still be influenced by the scale of the investigation.

[30]In our initial step, we use a 1D-homogenous SCAL approach to extract the relative permeability from the larger-scale USS experiments. To achieve this, we first simulate the displacement process, utilizing the 'true' SCAL saturation functions applicable to the same rock type, as per [30]. Subsequently, we perform a history match of the experimental data to determine $k_r(S_w)$, using $P_c(S_w)$ derived from MICP, data that is usually available for standard core analysis. To apply the MICP curve to primary drainage, we perform a scaling operation based on the interfacial tension (IFT) as follows:

$$P_c(\sigma) = \frac{\sigma}{\sigma_{ref}}\, p_{c,ref}, \qquad (1)$$

where σ_{ref} is the mercury-air IFT (480 mN/m) and σ is the IFT of the decane- and CO_2-brine systems, which is assigned 45 mN/m and 40 mN/m [35], respectively. Furthermore, we apply the closure correction to MICP based on the methodology presented by [36]. The pressure drop and the production data were then matched by varying $k_r(S_w)$. The MICP-scaled $P_c(S_w)$ for decane-brine, in comparison with the data derived from SCAL measurements, is examined in [30]. This is depicted in **Fig. 4** (c) and (f) for both decane-brine and CO_2-brine systems. Except for the entry pressure, the scaled MICP curve falls well within the uncertainty range of the SCAL data.

The SCAL interpreted $k_r(S_w)$ and $P_c(S_w)$ from [30] can now be directly compared to the decane-brine USS flooding experiments since both refer to the same rock-fluid system. There is a large deviation between the predicted and observed results; the pressure drop and the brine production curve are strongly underestimated, as indicated in **Fig. 3** (a) and (b) – the SCAL data are not directly applicable to the investigated scale.

A good match can be achieved by history matching the experimental data. For this, $k_r(S_w)$ is parametrized using the two commonly used representations, namely, Corey [37] and LET [38]. Since the experimental process is primary drainage, the residual decane saturation and the respective endpoints were fixed to $S_w = 1$ and $k_{rw}(S_w = 1) = 1$ using Corey, and all other parameters of $k_r(S_w)$ were open for matching. The matched experimental pressure drop, production curve and saturation profiles are shown in the top row of **Fig. 3**. Even if the saturation profiles simulated on a homogeneous domain cannot reflect the experimental profiles, ΔP and the cumulative brine production are matched well with some deviations in the transient part and specifically at the breakthrough point.

The LET parametrization is used as a second attempt to match the experimental measurements using a 1D homogeneous model, which offers greater flexibility at the expense of more fitting parameters. For uncertainty analysis, we used MCMC simulations, the same methodology as applied to the SCAL experiments in [30]. Note that in the present case, $P_C(S_w)$ is kept constant to the scaled MICP mentioned before.

The history match results and the quantified uncertainty ranges are shown in **Fig. 4**, along with the best match from the SCAL interpretation in **Fig. 4** (a) and (b). The LET matches the experimental data perfectly. In comparison to the SCAL reference data, however, Corey $k_r(S_w)$ generally shows a lower mobility of both phases, while LET shows a crossover with higher mobilities at high phase saturations and lower mobility at lower phase saturations. In any case, the differences between SCAL and the larger scale homogeneous interpretations are not subtle but substantially out of the given confidence interval of the SCAL data [30] and the USS data given for the LET parametrization. The saturation profiles show a poor match as expected; specifically, a homogenous simulation domain cannot represent a heterogeneous rock sample, but the brine production curve's overall material balance is met.

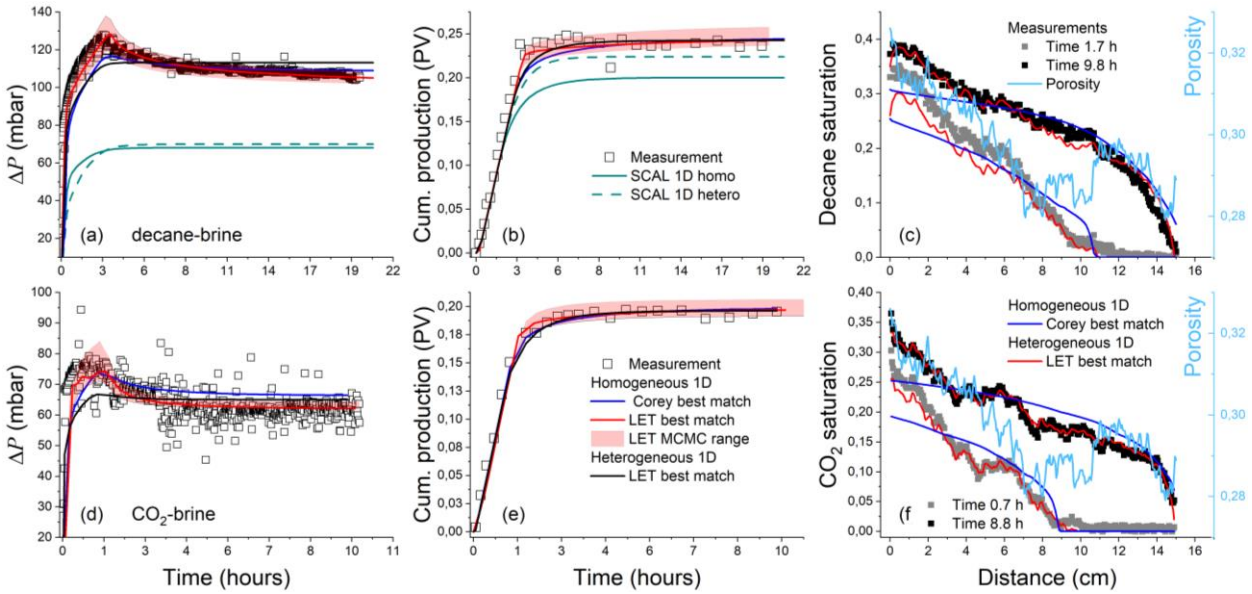

Fig. 3. Comparative Analysis of Experimental and Numerical Interpretations of Decane-Brine and CO_2-Brine Displacement Tests in Homogeneous Domains. This figure presents the comparison between experimental outcomes (depicted by symbols) and their corresponding numerical interpretations for both decane-brine (upper row) and CO_2-brine (lower row) displacement tests. From left to right, the panels show: (a) the pressure differential, (b) the brine production curve over time, and (c) the decane and CO_2 saturation profiles at two distinct time intervals as indicated in the legend. The solid lines in each graph represent the 1D numerical history-matching outcomes using homogeneous and heterogeneous simulation domains based on the CT density profile (represented by the light blue line). The models used for the relative permeability calculations and their respective uncertainty intervals are highlighted in the legend and elaborated upon in the main text. Consistent coloring and symbols are utilized across all figures to enhance comprehension. For example, the blue line labelled 'Corey best match' in figure (e) retains the same meaning in all related figures.

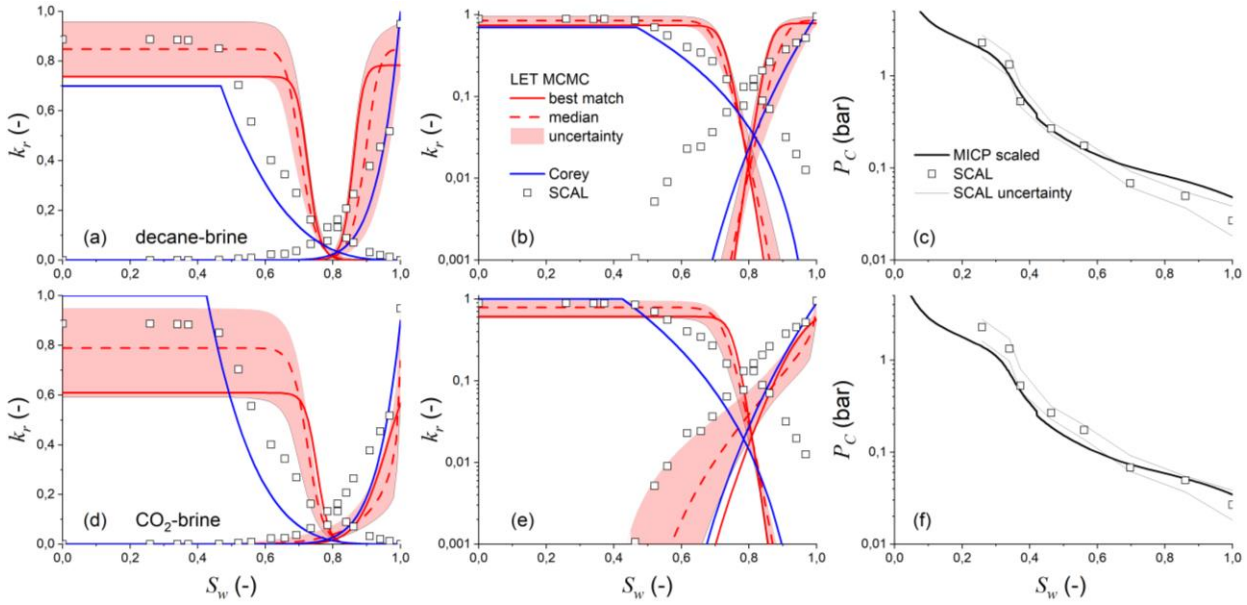

Fig. 4. Comparative Analysis of Relative Permeability and Capillary Pressure Saturation Functions in Decane-Brine and CO_2-Brine Displacement Experiments in Homogeneous Domains. This figure shows the results of history matching performed on 1D homogenous and 1D heterogeneous simulation domains, utilizing capillary pressure functions (shown on the right) as input. The top panels (a) to (c) represent the history matching (HM) results for the decane-brine experiments, while the lower panels (d) to (f) showcase the results from the CO_2-brine displacement experiments. From left to right, each panel depicts: relative permeability k_r presented in both linear and logarithmic scales, and capillary pressure P_c on a logarithmic scale. The squares in each panel correspond to SCAL results, which are measured on a smaller, homogenous scale. Consistent symbols and colors are used throughout the figure to ensure ease of understanding and coherence.

The same procedure was applied to the CO_2-brine displacement experiment, as shown in the lower row in **Fig. 2** and **Fig. 3**. Additionally, here, we applied a homogeneous 1D simulation domain and Corey and LET parametrization of the relative permeability to be matched. The MICP curve was scaled in the same way with an IFT of 40 mN/m and a contact angle of 140 as representative of the CO_2-Brine fluid pair [34].

By history matching, good matches similar to the decane-brine case could be achieved with the advantage of the LET model. The data are shown in **Fig. 3** (d) and (e). The MCMC confidence interval (P10 to P90) covers the experimental data points well. The respective saturation profiles for two subsequent time steps are shown in **Fig. 3** (f). Again, the complexity of the experimental saturation profile cannot be matched, but the material balance is honored.

The resulting $k_r(S_w)$ values are shown in **Fig. 4** (d) and (e). Compared to the decane-brine system, the relative CO_2-brine permeability shows a significant difference in water mobility, which is initially smaller but decreases significantly less with increasing CO_2 saturation than in the reference system. Furthermore, compared to the reference case, the uncertainty from the MCMC analysis (P10 to P90) is significantly lower for the brine relative permeability but higher for the CO_2 phase.

From these observations, we conclude that (a) HM complex experimental data with a 1D homogeneous simulation domain allow a perfect description of the experimental ΔP and the brine production curve using a flexible $k_r(S_w)$ parametrization. (b) The simulated saturation profiles $S_w(x)$ do not match the complex experimental profiles but match the material balance as a result of the assumed homogeneity. (c) By assuming homogeneity, $k_r(S_w)$ represents the average sample volume and may therefore be considered upscaled.

4 Introducing Heterogeneity

To model the heterogeneous saturation profiles, as presented in **Fig. 3** (c) and (f), the methodology presented by [7] is used. The authors characterize core heterogeneity by scaling the capillary pressure in the grid block. In the methodology implemented here, the 1D simulation domain is divided into 2-mm-size slices, which captures the sample heterogeneity with considerable detail. Each grid (j) is assigned a distinct value for capillary pressure $P_c^j(S)$, porosity ϕ_j, and absolute permeability K_j. Small-scale variations in fluid saturation by capillary heterogeneity can be quantified through variations in capillary entry pressure for each grid element in the system [7]. In Brooks-Corey parametrization [37], this entry pressure is denoted as P_d; therefore, we have:

$$P_c^j(S) = \frac{1}{f_j} P_c(S) = \frac{P_{dj}}{P_d} P_c(S) \quad j = 1, \dots, N, \qquad (2)$$

where f_j is the scaling factor, N is the number of elements in the system and P_{dj} is the entry pressure for the jth element. $P_c(S)$ is the reference capillary pressure curve, which is measured experimentally by MICP or by history matching SCAL experiments. To consider heterogeneity, we use Brooks-Corey parametrization for the reference capillary pressure, and we history match its parameters to calculate the system's capillary pressure. To calculate the spatial variations in porosity and absolute permeability, we use the Leverett-J function, $J(S)$, which states:

$$J(S) = \sqrt{K/\phi}\,\frac{P_c(S)}{\gamma} \qquad (3)$$

Analogous to the formulation for capillary scaling, we can write:

$$f_j = \frac{P_d}{P_{dj}} = \sqrt{\frac{K_j/\phi_j}{K_\mathrm{m}/\phi_\mathrm{m}}} \tag{4}$$

where K_j and ϕ_j are the absolute permeability and porosity for each grid element and K_m and ϕ_m are the experimentally measured average porosity and permeability of the core, respectively. For heterogeneous modeling, the steady-state saturation profile can be calculated using the equation below:

$$\frac{\mathrm{d}S}{\mathrm{d}x_\mathrm{D}} = \left(\frac{q\mu_\mathrm{nw}I}{AK_j}\right)\left(\frac{1}{k_\mathrm{r,nw}(S)}\right)\left(\frac{f_j}{\mathrm{d}P_\mathrm{c}(S)/\mathrm{d}S}\right), \tag{5}$$

in which we solve for the jth element of the system. This equation is similar to the one that we solve for homogeneous modeling, except f_j is multiplied by the last term of the equation. In the simulator developed for this purpose (based on MRST), a saturation number is assigned to each grid element, and the capillary pressure of each element is divided by the corresponding scaling factor f_j. To calculate the scaling factors, we minimize the following objective function:

$$E(x_j) = \sum_{k=1}^{N_\mathrm{q}} \left(\frac{P_\mathrm{c}\left(S^\mathrm{exp}(x_j)\right) - f_j P_\mathrm{c}\left(S^\mathrm{H}(x_j)\right)}{P_\mathrm{c}\left(S^\mathrm{exp}(x_j)\right)}\right)^2, j = 1, \ldots, N, \tag{6}$$

where P_c is the reference capillary pressure curve, f_j is the scaling factor, $S^\mathrm{exp}(x_j)$ is the slice average water saturation measured during the experiment, and $S^\mathrm{H}(x_j)$ is the saturation profile calculated with homogeneous simulations. This approach is justified since the capillary pressure profile is almost unaffected by small-scale heterogeneities [7].

Having calculated the scaling factors using equation (6), we then calculate K_{hm} using equation (4) and the porosity profile shown in **Fig. 3** (c). Therefore, for heterogeneous modeling, each grid cell has three distinct properties, namely, porosity ϕ, absolute permeability K (calculated from equation (4)), and capillary scaling factor f (calculated using equation (6))

The numerical responses of the pressure difference ΔP, brine production Q, and saturation profiles $S(x)$ are then history matched to the experimental measurements using a multiobjective error function that is minimized using the genitive algorithm from the MATLAB optimization toolbox:

$$I = \frac{1}{N}\sum_{j=1}^{N}\left(\frac{\Delta P^\mathrm{sim}(x_j) - \Delta P^\mathrm{exp}(x_j)}{\Delta P^\mathrm{exp}(x_j)}\right)^2$$
$$J = \frac{1}{N}\sum_{j=1}^{N}\left(\frac{Q^\mathrm{sim}(x_j) - Q^\mathrm{exp}(x_j)}{Q^\mathrm{exp}(x_j)}\right)^2 \tag{7}$$
$$K = \frac{1}{N}\sum_{j=1}^{N}\left(\frac{S^\mathrm{sim}(x_j) - S^\mathrm{exp}(x_j)}{S^\mathrm{exp}(x_j)}\right)^2.$$

In the methodology presented by [7], the capillary pressure scales are calculated from steady-state drainage experiments, in which the saturation profiles at the end of each fractional flow were evaluated. The novelty of the methodology presented here is the analysis of single-rate drainage experiments. For this purpose, the scaling factors are calculated from one saturation profile at the transient state and one at the steady state, i.e., late in the injection period.

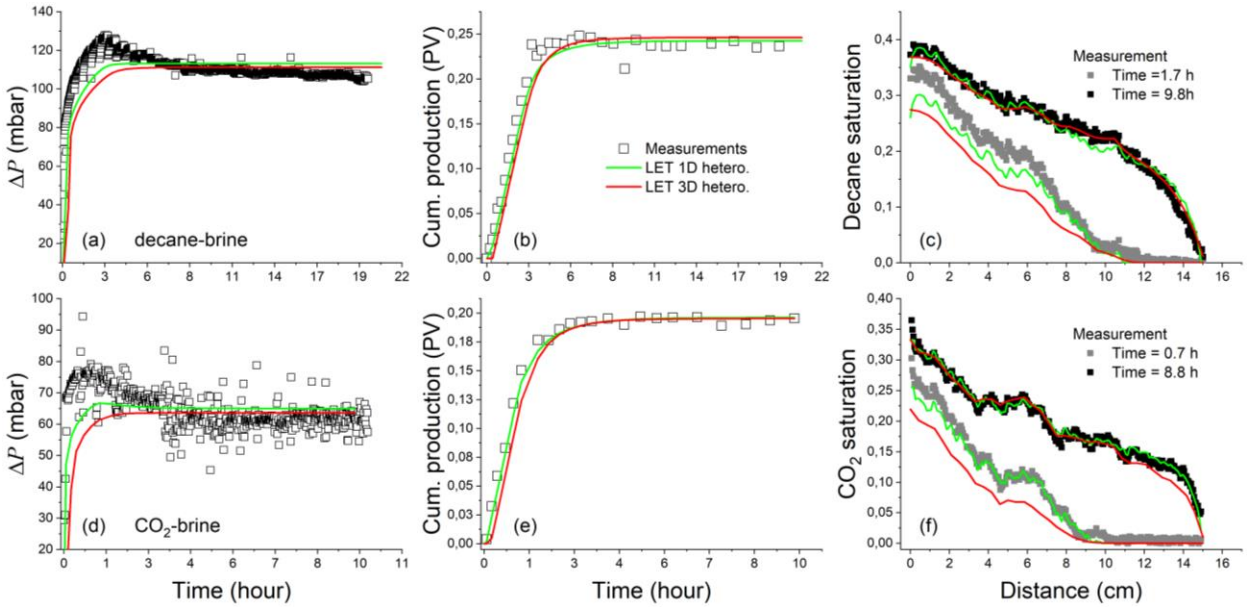

Fig. 5. Comparative Analysis of Experimental and Numerical Results in Decane-Brine and CO_2-Brine Displacement Experiments Considering Heterogeneity. The top and bottom rows represent the experimental responses (indicated by symbols) for decane-brine and CO_2-brine displacement experiments, respectively, and their corresponding numerical interpretation similar to **Fig. 3**. From left to right, each panel depicts: the pressure difference and brine production curves over time, and saturation profiles for decane and CO2 at two subsequent time steps as specified in the legend. The lines in each panel represent the results from the numerical history-matching process utilizing a 1D heterogeneous domain derived from the CT density profile and the full 3D heterogeneous volume. The employed relative permeability models are indicated in the legend and discussed in detail in the main text. This figure demonstrates the integration of heterogeneity in modeling the displacement experiments.

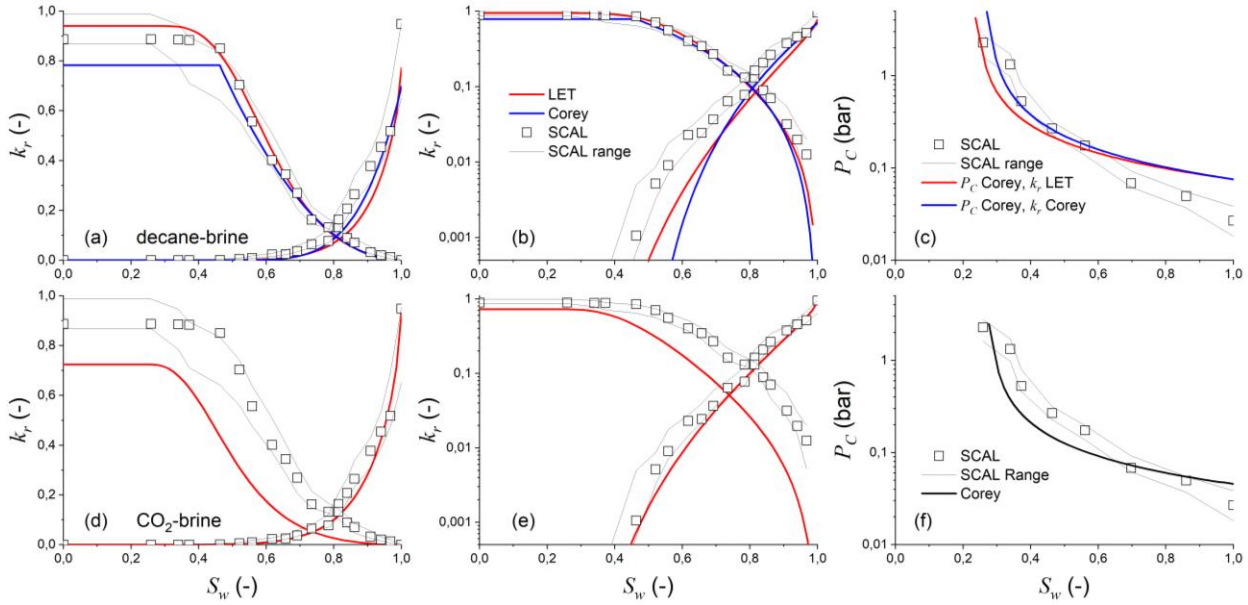

Fig. 6. Comparative Visualization of Relative Permeability and Capillary Pressure Saturation Functions in Heterogeneous Domains. This figure showcases the outcomes of history matching processes applied on the 1D and 3D heterogeneous simulation domains, derived from decane-brine and CO_2-brine displacement experiments. The top row panels (a) to (c) exhibit the history-matching results for the decane-brine experiments, whereas the bottom row panels (d) to (f) represent the outcomes for the CO_2-brine displacement experiments. Each set of panels, from left to right, display: relative permeability k_r on both linear and logarithmic scales, and capillary pressure P_c on a logarithmic scale. The squares in each graph correspond to the SCAL results that were obtained from measurements on a smaller scale deemed as homogeneous. This figure aids in contrasting and understanding the impact of heterogeneity on relative permeability and capillary pressure functions.

5 Interpretation Considering the 1D Porosity Profile

With the above discussed model, we implement porosity, permeability and capillary heterogeneity in the 1D simulation domain. The match of a forward simulation using the SCAL interpreted $k_r(S_w)$ and $P_c(S_w)$ [30] is shown in **Fig. 3** (a) and (b). It shows that, even when the simulations are performed on the heterogeneous modeling domain, the $k_r(S_w)$ and $P_c(S_w)$ interpretation from SCAL lead to large deviations in ΔP, the brine production is underestimated and the saturation profiles cannot be matched.

The match of the experimental responses for decane-brine (top row) and CO_2-brine (bottom row) are shown in **Fig. 5**. By including the exact porosity profile, more experimental data have to be described with only a few additional parameters, such as the scaling factor. This is at the expense of the quality of the agreement of the numerical interpretation with the experimental data, as shown in **Fig. 5**. The saturation profiles and the brine production curve are now satisfactorily described. However, the pressure difference ΔP shows that the transient part around the breakthrough time cannot be described exactly, which is also visible in the agreement with the other experimental responses.

The resulting Corey and LET $k_r(S_w)$ and Brooks-Corey $P_c(S_w)$ are shown together with the SCAL interpretations in **Fig. 6**; including the heterogeneity in the simulations causes the resulting $k_r(S_w)$ to come ultimately close to the uncertainty range predicted from the SCAL interpretation by [30]. The predicted brine $k_r(S_w)$ for both fluid pairs is just at the lower boundary of the uncertainty range, but the decane $k_r(S_w)$ is well inside the uncertainty interval. The largest deviation shows the calculated CO_2 k_r, which is substantially lower than the SCAL predictions. However, the SCAL experiments refer to the decane-brine system rather than to CO_2-brine and may be caused by different wetting properties. The good agreement of the simulation and experiment demonstrates the following: (a) the methodology developed by [7] is applicable to a single-rate USS drainage experiment, and (b) including the heterogeneity results in $k_r(S_w)$ saturation functions that come close to the formerly called "true" $k_r(S_w)$, as obtained from classical SCAL experiments. However, as the comparison with the homogeneous simulations shows, this "true" $k_r(S_w)$ is just meaningful if the heterogeneity is explicitly described.

The calculations of the scaling factors and Pareto fronts from the optimization method used show a linear trend between the error from production and the error from the saturation profile. This addresses the inconsistency observed in the homogeneous simulations and confirms the need for heterogeneous simulations for the EST core plug.

6 3D Heterogeneous Modeling

6.1 Converting medical-CT data to 3D saturation maps

The 3D porosity and saturation maps were calculated from medical CT scans. The underlying grayscale images are given in absolute Hounsfield units (HU). The images were processed by median and Gaussian-Blur-3D filtering to reduce noise within the gathered scans and to enhance the contrast between the fluid phases.

The 3D porosity map was derived from difference imaging, i.e., taking the difference between the brine-saturated scan and the dry scan, as suggested by [39–41]. The 3D porosity profile was obtained by using a voxel-by-voxel approach:

$$\phi(\vec{x}) = \frac{HU^{sat}_{brine}(\vec{x}) - HU_{dry}(\vec{x})}{HU_{brine} - HU_{air}} = \alpha \cdot \left(HU^{sat}_{brine}(\vec{x}) - HU_{dry}(\vec{x})\right), \quad (8)$$

where $HU^{sat}_{brine}(\vec{x})$ refers to the scan of the fully brine-saturated sample, $HU_{dry}(\vec{x})$ to the dry scan, and HU_{brine} and HU_{air} correspond to the HU values of brine and air. To achieve the best calibration, the difference scan is scaled by the factor α to match the standardly measured porosity of the plug.

Consequently, the 3D fluid distributions were calculated as a function of space and time from the dynamic CT profiles, $HU_{exp}(\vec{x}, t)$ by equation (9):

$$S_{CO_2}(\vec{x}, t) = \frac{HU^{sat}_{brine}(\vec{x}, t_0) - HU_{exp}(\vec{x}, t)}{HU^{sat}_{brine}(\vec{x}) - HU^{sat}_{CO_2}(\vec{x})}, \quad (9)$$

where $HU^{sat}_{brine}(\vec{x}, t_0)$ and $HU_{exp}(\vec{x}, t)$ correspond to the initial scan at $S_w = 1$ and the current experimental time step, respectively, and $HU^{sat}_{CO_2}(\vec{x})$ is the scan of the fully CO2-saturated sample. The two calibration scans in the denominator were conducted prior to the flooding experiment. The experimental and simulated 3D saturation profiles are shown in **Fig. 7** (a) to (f).

The original resolution of the CT images is 0.18×0.18×0.5 mm3. For computational efficiency, we binned 24×24×8 voxels, which means that each grid block measures approximately 4 mm cubed. To analyze the sensitivity of the simulation results to the choice of binning, simulations were performed with a lower binning of 12×12×4 for the decane-brine case. Since the effect of downscaling on the results was found to be minimal and since the simulation time increases exponentially with the number of grid blocks, a binning of 24×24×8 was used for the majority of the simulations.

6.2 3D Heterogeneous Modeling

The methodology of capillary pressure scaling can be extended from 1D to 3D simulation domains [29]; the principle of calculating the scaling factor is the same as that for 1D but is calculated on the 3D grid. Because of the computational demand, it is not possible to history match the experimental data in 3D since each simulation usually takes around four hours. Instead, we forward simulate the displacements using the best match – the LET $k_r(S_w)$ case – obtained from the 1D heterogeneous model and statistically compare the simulated and experimental responses on fluid saturation.

The measured and predicted saturation distributions are shown in **Fig. 7** (a) and (b) for the decane-brine and (e) and (f) for CO_2-brine displacement. For better comparison, the 1D projection, i.e., the resulting 1D saturation profiles, are plotted in **Fig. 5** (c) and (f) together with the experimental and 1D-derived saturation profiles. The match of the 3D results to the 1D and experimental projected saturation profiles is reasonable, considering that it is not the result of a history match but a forward simulation. The ΔP and the cumulative brine production are comparable to the responses of the 1D heterogeneous results with the same limitations around the breakthrough time, as discussed previously. This may be a limitation of the capillary pressure scaling method, as one of the underlying assumptions of the methodology is that the system is in a steady state [7, 42].

To better quantify the saturation profile, **Fig. 7** (c) to (h) shows a statistical comparison of the experimentally determined and numerically simulated 3D saturation profiles presented in **Fig. 7** (a) and (b). (c) and (g) show the respective histograms for the decane-brine saturation state after 9.8 h and the CO_2-brine saturation state after 8.8 h of flooding. The data show a perfect match over a wide saturation range, which is further quantified in the respective correlation plots (d) and (h), which are obtained by plotting the simulated saturation of each grid block versus the experimentally measured saturation. The data show a high degree of correlation with correlation coefficients above 0.99 and 0.98 for the decane and CO_2 cases, respectively. Deviations in the experimentally and numerically derived histograms and hence in the correlations are predominantly at high-brine phase saturations, where the experimental data show saturations above one, which is an error in the measurements. However, the affected range is not relevant for fluid displacement physics.

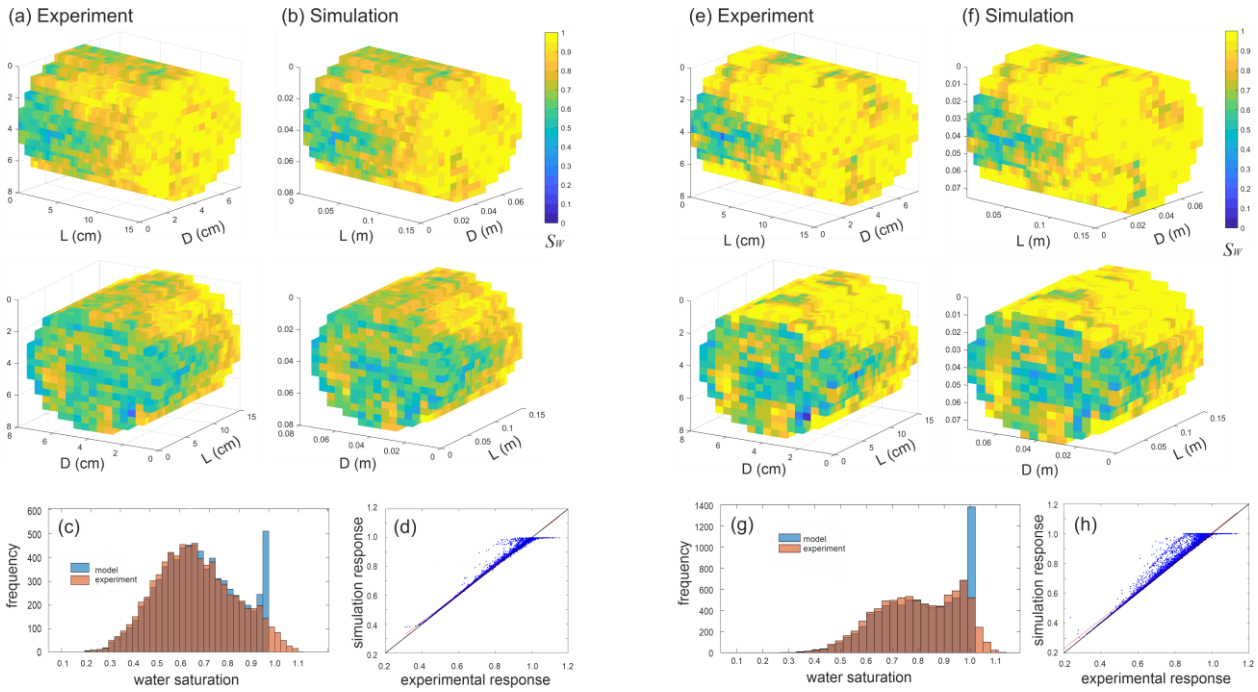

Fig. 7. (a) Measured 3D water saturation profiles after 9.8 h of decane flooding. The flow direction is from left to right. (b) Corresponding simulation output. (c) Comparative experimental and simulated water saturation histograms and (d) correlation between simulated and experimentally measured saturations. The black line indicates the slope of unity with zero intercept. The red line shows a linear regression to the data. Figures (e) to (h) show the same data after 8.9 h of CO2 flooding.

7 Discussion and Conclusions

In a first attempt to interpret the experimental data, we proceeded as in a classical SCAL workflow and assumed the simulation domain to be one-dimensional and homogeneous. This has the advantage that the stochastic analysis is the same as that for the SCAL data, which is numerically too costly for heterogeneous systems that are in three dimensions. A simple forward simulation using the SCAL data cannot describe the experimental data on the next larger scale with a 12× larger volume. However, good agreement can be achieved by varying the relative permeability except for the complex saturation profile, which cannot be described in the frame of a homogeneous model. This, of course, has the consequence that the relative permeability curves extracted from both scales do not match.

Consideration of the 1D porosity profile and the corresponding permeability and capillary scaling is the first step in capturing the influence of heterogeneity on two-phase flow. However, the use of SCAL data in forward modeling still leads to a discrepancy between simulation results and experimental responses. However, the experiments can again be matched by optimizing the $k_r(S_w)$ saturation functions; for the decane-brine system, the experimental responses, including the saturation profiles, are well described. The extracted $k_r(S_w)$ and $P_c(S_w)$ are close to the SCAL k_r and scaled MICP P_c. A similar picture can be drawn for the CO_2-brine displacement, but the relative CO_2 permeability, i.e., CO_2 mobility, is significantly lower with respect to the SCAL standard. However, the data are trustworthy since the SCAL data refer to the decane-brine displacement and the CO_2-brine system may have different wetting behaviors.

To verify the approach of heterogeneity implementation, the displacements were forward simulated in the 3D heterogeneous domain using $k_r(S_w)$ and $P_c(S_w)$ of the best match of the 1D heterogeneous model. For both systems, the numerical and experimental saturation states show very good correlation. The heterogeneous models, even providing a good overall description of USS experiments, experience deviations from the experimental data around the breakthrough time, as evident in all experimental responses. The exact reason for this deviation is still an open question and is under investigation.

In this article, the challenges of interpreting multiphase flow experiments on laboratory samples of rocks with mm-scale heterogeneities are discussed. Practically, it is not yet possible to implement such small-scale heterogeneity in reservoir simulations where it would be on a subgrid scale. The proof that the classic SCAL-derived relative permeability is only valid when considering small-scale heterogeneity makes SCAL application in reservoir simulation questionable. This is especially true for multiscale-heterogeneous carbonates and CO_2-brine displacements with its unfortunate mobility contrast. For such complex rocks, new concepts are needed. A better choice would be the naturally upscaled result of the 1D homogeneous interpretation, which describes the system on the scale of investigation. However, such data cannot be extracted from standard SCAL measurements as performed in the frame of field developments and may still be scale dependent.

Our results demonstrate that simple USS experiments can be used to investigate the influence of capillary heterogeneity on $k_r(S_w)$ which is specially valuable for CO_2 research since CO_2 steady state experiments are extremely demanding in terms of maintaining fluid phase equilibria during the experiment. It further shows that a rigorous upscaling

procedure including rock heterogeneity on various scales is needed to use standard workflows such as special core analysis for CCS developments in carbonates.

References

1. Aminu MD, Nabavi SA, Rochelle CA, Manovic V (2017) A review of developments in carbon dioxide storage. Appl Energy 208:1389–1419
2. Onoja MU, Shariatipour SM (2019) Assessing the impact of relative permeability and capillary heterogeneity on Darcy flow modelling of CO2 storage in Utsira Formation. Greenhouse Gases: Science and Technology 9:1221–1246
3. Hosseini SA, Lashgari H, Choi JW, Nicot J-P, Lu J, Hovorka SD (2013) Static and dynamic reservoir modeling for geological CO2 sequestration at Cranfield, Mississippi, U.S.A. International Journal of Greenhouse Gas Control 18:449–462
4. Lu J, Kordi M, Hovorka SD, Meckel TA, Christopher CA (2013) Reservoir characterization and complications for trapping mechanisms at Cranfield CO2 injection site. International Journal of Greenhouse Gas Control 18:361–374
5. Ringrose PS, Sorbie KS, Corbett PWM, Jensen JL (1993) Immiscible flow behaviour in laminated and cross-bedded sandstones. J Pet Sci Eng 9:103–124
6. Zhang D, Zhang R, Chen S, Soll WE (2000) Pore scale study of flow in porous media: Scale dependency, REV, and statistical REV. Geophys Res Lett 27:1195–1198
7. Hosseinzadeh Hejazi SA, Shah S, Pini R (2019) Dynamic measurements of drainage capillary pressure curves in carbonate rocks. Chem Eng Sci 200:268–284
8. Georgiadis A, Berg S, Makurat A, Maitland G, Ott H (2013) Pore-scale micro-computed-tomography imaging: Nonwetting-phase cluster-size distribution during drainage and imbibition. Phys Rev E 88:033002
9. Chang J, Yortsos YC (1992) Effect of Capillary Heterogeneity on Buckley-Leverett Displacement. SPE Reservoir Engineering 7:285–293
10. Reynolds CA, Krevor S (2015) Characterizing flow behavior for gas injection: Relative permeability of CO2-brine and N2-water in heterogeneous rocks. Water Resour Res 51:9464–9489
11. Kuo C-W, Benson SM (2015) Numerical and analytical study of effects of small scale heterogeneity on CO2/brine multiphase flow system in horizontal corefloods. Adv Water Resour 79:1–17
12. Jackson SJ, Agada S, Reynolds CA, Krevor S (2018) Characterizing Drainage Multiphase Flow in Heterogeneous Sandstones. Water Resour Res 54:3139–3161
13. Wenck N, Jackson SJ, Manoorkar S, Muggeridge A, Krevor S (2021) Simulating Core Floods in Heterogeneous Sandstone and Carbonate Rocks. Water Resour Res. https://doi.org/10.1029/2021WR030581
14. Berg S, Oedai S, Ott H (2013) Displacement and mass transfer between saturated and unsaturated CO2–brine systems in sandstone. International Journal of Greenhouse Gas Control 12:478–492
15. Jackson SJ, Krevor S (2020) Small-Scale Capillary Heterogeneity Linked to Rapid Plume Migration During CO Storage. Geophys Res Lett. https://doi.org/10.1029/2020GL088616
16. Egermann P, Lenormand R (2005) A New Methodology to Evaluate the Impact of Localized Heterogeneity on Petrophysical Parameters (kr, Pc Applied to Carbonate Rocks. Petrophysics - The SPWLA Journal of Formation Evaluation and Reservoir Description 46:
17. Renard Ph, de Marsily G (1997) Calculating equivalent permeability: a review. Adv Water Resour 20:253–278
18. Reynolds CA, Blunt MJ, Krevor S (2018) Multiphase Flow Characteristics of Heterogeneous Rocks From CO2 Storage Reservoirs in the United Kingdom. Water Resour Res 54:729–745
19. Pini R, Benson SM (2013) Simultaneous determination of capillary pressure and relative permeability curves from core-flooding experiments with various fluid pairs. Water Resour Res 49:3516–3530
20. Pini R, Benson SM (2013) Characterization and scaling of mesoscale heterogeneities in sandstones. Geophys Res Lett 40:3903–3908
21. Ni H, Boon M, Garing C, Benson SM (2019) Predicting CO2 residual trapping ability based on experimental petrophysical properties for different sandstone types. International Journal of Greenhouse Gas Control 86:158–176
22. Kong X, Delshad M, Wheeler MF (2015) History Matching Heterogeneous Coreflood of CO2/Brine by Use of Compositional Reservoir Simulator and Geostatistical Approach. SPE Journal 20:267–276
23. Krause MH, Benson SM (2015) Accurate determination of characteristic relative permeability curves. Adv Water Resour 83:376–388
24. Krause M, Perrin J-C.-C, Benson SM. M (2011) Modeling Permeability Distributions in a Sandstone Core for History Matching Coreflood Experiments. SPE Journal 16:768–777
25. Krause M, Krevor S, Benson SM (2013) A Procedure for the Accurate Determination of Sub-Core Scale Permeability Distributions with Error Quantification. Transp Porous Media 98:565–588
26. Kuo C-W, Perrin J-C, Benson SM (2011) Simulation studies of effect of flow rate and small scale heterogeneity on multiphase flow of CO2 and brine. Energy Procedia 4:4516–4523
27. Berg S, Unsal E, Dijk H (2021) Non-uniqueness and uncertainty quantification of relative permeability

measurements by inverse modelling. Comput Geotech 132:103964

28. Berg S, Unsal E, Dijk H (2021) Sensitivity and Uncertainty Analysis for Parameterization of Multiphase Flow Models. Transp Porous Media 140:27–57
29. Kurotori T, Pini R (2021) A general capillary equilibrium model to describe drainage experiments in heterogeneous laboratory rock cores. Adv Water Resour 152:103938
30. Amrollahinasab O, Azizmohammadi S, Ott H (2023) Simultaneous interpretation of SCAL data with different degrees of freedom and uncertainty analysis. Comput Geotech 105074
31. Ruspini LC, Øren PE, Berg S, et al (2021) Multiscale Digital Rock Analysis for Complex Rocks. Transp Porous Media 139:301–325
32. Burmester G, Zekiri F, Jurcic H, Arnold P, Ott H (2022) Integration and Upscaling of Multi-Phase Fluid Flow Properties in Clastic Reservoirs. In: 83rd EAGE Annual Conference & Exhibition. European Association of Geoscientists & Engineers, pp 1–5
33. Ott H, Pentland CH, Oedai S (2015) CO 2 –brine displacement in heterogeneous carbonates. International Journal of Greenhouse Gas Control 33:135–144
34. Leverett MC (1941) Capillary Behavior in Porous Solids. Transactions of the AIME 142:152–169
35. Georgiadis A, Maitland G, Trusler JPM, Bismarck A (2010) Interfacial Tension Measurements of the (H2O + CO2) System at Elevated Pressures and Temperatures. J Chem Eng Data 55:4168–4175
36. McPhee C, Reed J, Zubizarreta I (2015) Core analysis: a best practice guide. Elsevier
37. R. H. Brooks and A. T. Corey (1964) Hydraulic Properties of Porous Media and Their Relation to Drainage Design. Transactions of the ASAE 7:0026–0028
38. Lomeland F, Ebeltoft E, Thomas WH (2005) A new versatile relative permeability correlation. International symposium of the society of core analysts, Toronto, Canada 112:
39. Ott H, de Kloe K, van Bakel M, et al (2012) Core-flood experiment for transport of reactive fluids in rocks. Review of Scientific Instruments 83:084501
40. Wellington SL, Vinegar HJ (1987) X-ray computerized tomography. https://doi.org/10.2118/16983-PA
41. Ott H (2015) CO2-brine primary displacement in saline aquifers: experiments, simulations and concepts. Habilitationsschrift, RWTH Aachen
42. Pini R, Krevor SCM, Benson SM (2012) Capillary pressure and heterogeneity for the CO2/water system in sandstone rocks at reservoir conditions. Adv Water Resour 38:48–59